Research Article

Baboucarr Ceesay, Muhammad Z. Baber, Nauman Ahmed, Siegfried Macías, Jorge E. Macías-Díaz*, and María G. Medina-Guevara

Solitonic wave solutions of a Hamiltonian nonlinear atom chain model through the Hirota bilinear transformation method

https://doi.org/10.1515/phys-2025-0150
received January 21, 2025; accepted March 29, 2025

Abstract: This study employs the Hirota bilinear transformation method to investigate solitary and soliton solutions resulting from different symmetry wave functions associated with nonlinear atom chain models. These models are complex dynamic systems that have an impact on a variety of scientific areas. In this work, we derive exact solutions for several symmetry wave functions. Our results reveal a wide range of wave structures, including anti-kink waves (resulting from the interaction of exponential wave functions), M-shaped waves with single and double kinks (generated by combining M-shaped and kink wave functions), and periodic multiple lump waves (produced by the interaction of multi-lump and periodic wave functions). Solitary waves and numerous periodic lump waves have also been reported as a result of various multi-wave function combinations. In the present report, we also derive periodic bright lump waves, periodic cross-kink waves, and dark lump strip waves caused by interactions between exponential, trigonometric, and hyperbolic functions. Additional solutions include solitary waves from mixed wave functions and bright breather waves obtained from homoclinic breather functions. For illustration purposes, we provide three-dimensional visualizations of these solutions as well as accompanying contour plots.

Keywords: nonlinear atomic chain model, solitary wave solutions, soliton solutions, Hirota bilinear transformation method

*** Corresponding author: Jorge E. Macías-Díaz,** Department of Mathematics and Didactics of Mathematics, Tallinn University, Tallinn, Estonia; Department of Mathematics and Physics, Autonomous University of Aguascalientes, Aguascalientes, Mexico, e-mail: jemacias@correo.uaa.mx
Baboucarr Ceesay: Mathematics Unit, The University of The Gambia, Serrekunda, Gambia; Department of Mathematics and Statistics, The University of Lahore, Lahore, Pakistan
Muhammad Z. Baber: Department of Mathematics and Statistics, The University of Lahore, Sargodha Campus, Sargodha, Pakistan
Nauman Ahmed: Department of Mathematics and Statistics, The University of Lahore, Lahore, Pakistan
Siegfried Macías: University Center of Lagos, University of Guadalajara, Guadalajara, Mexico; Department of Mathematics and Physics, Autonomous University of Aguascalientes, Aguascalientes, Mexico
María G. Medina-Guevara: University Center of Lagos, University of Guadalajara, Guadalajara, Mexico

1 Introduction

Nonlinear partial differential equations (NLPDEs) are one of the primary approaches in the modeling and analysis of numerous complex processes [1–3]. These processes include, but are not limited to, plasma physics [4], nonlinear optics [5], chemical kinetics [6], physics of condensed matter [7], and even certain aspects of biology [8]. The reason for this is that NLPDEs are able to catch the dynamics of complex systems with various independent variables. While linear equations possess the property of being relatively simple, NLPDEs embrace the complexities existing within the natural and artificial systems. In this context, one avenue of investigation in NLPDEs is the search for exact solutions which can be used to interpret some physical reality. To that end, many different analytical and numerical approaches have been suggested. Some of the most notable methods involve the modified exp-function method [9], the modified generalized Kudryashov method [10], the extended Jacobi elliptic function rational expansion method [11], Riccati's equation expansion method [12], the sine-Gordon expansion method [13], the $\frac{G'}{G}$-expansion technique [14], the F-expansion approach [15], the Sardar sub-equation scheme [16], the Darboux transformation technique [17], the bilinear convolutional neural network method [18], the natural transform decomposition method [19], the modified fractional homotopy technique [20], the Laplace decomposition method [21], the Adomian decomposition method [22], the perturbation method [23], and the bilinear residual network method [24]. These

approaches are useful for integrable classes of some NLPDEs. However, some of these methods do not provide a generalized approach that can be used for any nonlinear problem. Therefore, there is always an urge to modify the existing methods or come up with new ones that can help in solving more difficult equations.

Among the multiple existing techniques, the Hirota bilinear transformation technique has received special emphasis in view of its application on many complex integrable NLPDEs. This technique is used to convert NLPDEs to bilinear equations, which are easier to deal with. This method allows us to derive soliton solutions, which play an important role in most systems. In the present work, the Hirota bilinear method is used to study solitary and soliton waves in a nonlinear atom chain (NAC) model. It is worth recalling that soliton theory, which is primarily concerned with solitary waves and their propagation, has been quickly established as one of the cornerstones of modern nonlinear physics and mathematics. Solitary waves are a class of waves that can propagate in certain media without changes due to dispersion. These waves propagate and keep their speed for a long time, which is an optimal condition for these waves to be used in describing localized physical processes, such as energy propagation in crystals [25], strain in crystal [26], as well as wave motion in a solid state [27]. Solitary waves have been studied by scientists in many contexts, including aqueous flows, light in fibers, and mechanical waves. For example, some reports investigate solitonic rogue waves induced by the modulation instability in a split-ring-resonator-based left-handed coplanar waveguide [28], (2 + 1)-dimensional variable coefficient equations in the investigation of oceanic solitons and localized wave solutions [29] and the effects of higher-order dispersion on solitary waves and modulation instability in a monomode fiber [30]. In addition, some reports investigate rogue wave dynamics in barotropic relaxing media [31], N-rotating loop-soliton solutions of the coupled integrable dispersionless equation [32], traveling wave-guide channels of a coupled integrable dispersionless system [33], and their scattering behaviors [34]. In other situations, solitons serve to study the stress, strain, and material responses of structures under different conditions [35–38].

Usually, the behavior of solitary waves is governed by NLPDEs, which are generally complex and often require advance techniques to solve them. What sets these equations apart from their linear counterparts is that they are frequently intractable. Instead, in order to obtain meaningful results, we need sophisticated analytical methods, such as the Hirota bilinear transformation approach or numerical approximations. In many industrial and scientific applications, systems are frequently affected by severe circumstances like high temperatures, high pressures, or fast deformation. The nonlinearities of these equations are essential for capturing those behaviors. Consequently, bettering the design and safety of mechanical systems requires an understanding of nonlinear equations. One area where NLPDEs have proven particularly valuable is in the modeling of NACs. These chains are widely used in the study of materials science and solid mechanics, as they provide insights into the behavior of materials at the atomic level [38–41]. NACs can model a variety of phenomena, including thermal conductivity, wave propagation, defect formation, and material deformation under stress [38,39]. By studying these chains, researchers may obtain a deeper understanding of how materials behave under extreme conditions, leading to the development of high-performance materials for various applications in science, engineering, and technology.

It is also important to point out that wave propagation and solitons in NACs have attracted attention in the last couple of years. In fact, several techniques have been designed to study them rigorously. For instance, Foroutan *et al.* [42] employed the extended trial equation technique and the improved Bernoulli sub-ordinary differential equation method to solve an NAC problem. They obtained trigonometric, soliton, hyperbolic, and kink solutions. These solutions have applications in generalized momentum for long-range interactions and Hamilton's equations. In order to analyze NACs, Junaid-U-Rehman *et al.* [46] made use of the Lie symmetry technique. They generated traveling-wave solutions and utilized the multiplier method to discover the conservation laws. Their results show the dynamics and patterns of the system. Shakeel *et al.* [47] applied the generalized auxiliary equation method to construct bright, periodic, singular, W-type, and M-type soliton solutions for the NAC model. Among many other reports available in the literature, these solutions form an important aspect in material and structural nanoscience.

On the other hand, the Hirota bilinear transformation technique has made significant contributions to our comprehension of the complex wave solutions produced by various NLPDEs. Notably, a number of researchers have used this technique in recent years to provide exact solutions to a range of NLPDEs. For instance, Ceesay *et al.* [48] employed the modified regularized long-wave equations to analyze the impact of different M-shaped waves in coastal environments. In order to obtain bilinear equations for NLPDEs with indeterminate coefficients, Yang and Wei [49] also applied Hirota's bilinear approach. By applying the tanh-coth and Hirota bilinear methods, Wazwaz [50] was able to find many solutions to the Sawada–Kotera–Kadomtsev–Petviashvili model. Furthermore, Rizvi *et al.* [51] used the Hirota bilinear approach to investigate saturated

ferromagnets. Khan and Wazwaz [52] also employed this technique using ansatz functions to derive numerous novel soliton solutions and multi-breather solutions for the Calogero–Bogoyavlenskii–Schiff (CBS) model, whereas Wang *et al.* [53] adopted a study of plasma and fluid dynamics for the generalized (3 + 1) Kadomtsev–Petviashvili model. Zhao *et al.* [54] also employed the bilinear approach to produce various lump, mixed lump-stripe solutions using the asymmetric (2 + 1) Nizhnik–Novikov–Veselov model. Using this method, Ren *et al.* [55] investigated the CBS-type system in the extended (2 + 1) dimensions. In turn, Rizvi and colleagues [56] investigated the coupled Higgs equations using the Hirota bilinear transformation method.

It is worthwhile mentioning that the Hirota bilinear approach extends beyond the traditional study of solitons, and gives margin to study other number of interesting wave forms (including rogue, singular, kink, anti-kink, breather, M-shaped, and lump waves). This fact demonstrates the method's broad application. These solutions (which are not just theoretical in nature) have real-world applications in fields like biomembrane, fluid dynamics, wave optical pulse, shallow water modeling, *etc*. Furthermore, given their significant advancements in our knowledge of waves and soliton solutions and their practical applications, these examples show the applicability of the Hirota bilinear technique across fields. In the present study, we departed from the Hirota bilinear transformation method and applied it to an NCA model. After examining earlier research conducted by different investigators who employed the NCA model, they reveal that the Hirota bilinear transformation techniques have not been applied to this system. The purpose of this study is to fill this vacuum in the research literature. In terms of originality, the present work derives novel solutions of an NAC model. Indeed, as some of the reviewers pointed out, there are already some solutions for particular NAC models reported in the literature. However, the investigation of NAC models with an associated Hamiltonian is a problem for which exact solutions have not been derived. Additionally, the Hirota bilinear transformation method has not been employed in those contexts. In that sense, the present work is one of the first in the literature, which tackles the derivation of analytical solutions for NAC models using the methodology proposed by Hirota.

2 Preliminaries

2.1 Physical model

The purpose of this subsection is to provide an overview of the NAC model under investigation. In our physical model, we will assume only one degree of freedom. The Hamiltonian of the system under study is provided by [42]

$$H = \sum_n \left[\frac{1}{2} m \dot{L}_n^{\,2} + \sum_{l \neq n} M(|L_n - L_l|) \right], \tag{1}$$

where $M(|L_n - L_l|)$ is the nonlinear potential, m is the mass of atom, and the dot represents the first derivative with respect to time. All functions depend only on the temporal variable, and the inner-most sum at the right-hand side of this equation takes into account only the nearest neighbors, that is, $l = n \pm 1$. Moreover, in what follows, we will consider the following potential function:

$$M(k_{nl}) = \frac{1}{12} k_{nl}^2 [6\alpha_i + 4\beta_i k_{nl} + \gamma_i k_{nl}^2]. \tag{2}$$

Here the relative displacement between the lth and the nth atoms is denoted by k_{nl}. The unique particle-to-particle interactions are displayed by index i. Recall that Hamilton's equations are given by

$$\begin{aligned} \frac{\partial H}{\partial L_n} &= -\dot{Q}_n, \\ \frac{\partial H}{\partial Q_n} &= \frac{\partial L_n}{\partial t} = \dot{L}_n. \end{aligned} \tag{3}$$

Applying Hamilton's equations to Eqs (1) and (2), we derive the approximate equation of motion

$$\begin{aligned} \frac{\mathrm{d}^2 L_n}{\mathrm{d}t^2} = {} & \alpha_1 (L_{n+1} - 2L_n + L_{n-1}) - \alpha_2 (L_{n+2} - 2L_n + L_{n-2}) \\ & + \beta_1 [(L_{n+1} - L_n)^2 - (L_n - L_{n-1})^2] \\ & + \beta_2 [(L_{n+2} - L_n)^2 - (L_n - L_{n-2})^2] \\ & + \gamma_1 [(L_{n+1} - L_n)^2 - (L_n - L_{n-1})^2] \\ & + \gamma_2 [(L_{n+2} - L_n)^2 - (L_n - L_{n-2})^2], \end{aligned} \tag{4}$$

where Q_n denotes the generalized momentum in Hamilton's equations. It is important to mention here that, in addition to chain atom models with long-range interactions [42], the present model is an extension of various other models studied in the literature. Some of them are models in which authors investigated the existence of dynamic solitary wave solutions [43], the presence of conservation laws using Lie analysis [44,45].

If the inter-atom spacing ε is sufficiently small to attain the continuum limit, then we can let $\varepsilon_n \to x$. As a result, we obtain the expansions

$$\begin{aligned} L_{n\pm1} = {} & L \pm \varepsilon L_x + \frac{1}{2!}\varepsilon^2 L_{xx} \pm \frac{1}{3!}\varepsilon^3 L_{xxx} + \frac{1}{4!}\varepsilon^4 L_{xxxx} \\ & \pm \frac{1}{5!}\varepsilon^5 L_{xxxxx} + \ldots \end{aligned} \tag{5}$$

and

$$L_{n\pm2} = L \pm 2\varepsilon L_x + \frac{4}{2!}\varepsilon^2 L_{xx} \pm \frac{8}{3!}\varepsilon^3 L_{xxx} + \frac{16}{4!}\varepsilon^4 L_{xxxx} \pm \frac{32}{5!}\varepsilon^5 L_{xxxxx} + \ldots. \tag{6}$$

Hence, Eq. (4) can be expressed as the NLPDE given by

$$L_{tt} - a^2 L_{xx} - bL_x L_{xx} - cL_x^2 L_{xx} - dL_{xxxx} = 0, \tag{7}$$

with the constants

$$a^2 = \frac{\varepsilon^2(\alpha_1 + 4\alpha_2)}{m}, \quad b = \frac{2\varepsilon^3(\beta_1 + 8\beta_2)}{m}, \quad c = \frac{\varepsilon^4(\gamma_1 + 16\gamma_2)}{m}, \quad d = \frac{\varepsilon^4(\alpha_1 + 16\alpha_2)}{12m}. \tag{8}$$

It is worthwhile to mention that Eq. (7) may find useful applications in the investigation of one-dimensional chains of atoms when they are studied from a microscopic point of view, in which case, the assumption that ε is sufficiently small is physically justified. In this study, we will apply the Hirota bilinear transformation approach and some *ansatz* functions to obtain various wave solutions for the NAC model given by Eq. (7).

2.2 Analytical method

At this stage, we recall the steps of the Hirota bilinear transformation method and apply them to solve Eq. (7) analytically. We start by applying the Cole–Hopf transformation, which is a logarithmic transformation for the dependent variable L, and we suppose that the solution to Eq. (7) is given by

$$L(x, t) = R(\ln(\Gamma(x, t)))_x, \tag{9}$$

where R is a constant to be determined. To find R, we begin by using the following function: $L(x, t) = e^{a_i x + \omega_i t}$. Here, a_i and ω_i represent wave numbers and dispersions, respectively. Substituting this equation in Eq. (7) yields the dispersion relation

$$\omega_i = a_i\sqrt{a^2 + da_i^2}. \tag{10}$$

As a consequence, it follows that

$$L(x, t) = e^{a_i x + a_i\sqrt{a^2 + da_i^2}t}. \tag{11}$$

We then consider the function $\Gamma(x, t) = 1 + e^{a_i x + a_i\sqrt{a^2 + da_i^2}t}$, and substitute it in Eq. (9). The result is then substituted in the linear part of Eq. (7), and then we solve for R to obtain $R = \frac{12d}{b}$ and $c = 0$. Hence, the logarithmic transformation becomes

$$L(x, t) = \frac{12d}{b}(\ln(\Gamma(x, t)))_x. \tag{12}$$

In this way, we transformed Eq. (7) into the bilinear form

$$(D_t^2 - a^2 D_x^2 - dD_x^4)\Gamma \cdot \Gamma = 0, \tag{13}$$

using transformation (12). Here the bilinear operator $D_x^u D_t^v$ is defined by

$$D_x^u D_t^v \Gamma \cdot \Lambda = \left(\frac{\partial}{\partial x} - \frac{\partial}{\partial x'}\right)^u \left(\frac{\partial}{\partial t} - \frac{\partial}{\partial t'}\right)^v \Gamma(x, t)\Lambda(x', t')|_{x=x', t=t'}. \tag{14}$$

Finally, we can write Eq. (13) as

$$-a^2\Gamma\frac{\partial^2\Gamma}{\partial x^2} + a^2\left(\frac{\partial\Gamma}{\partial x}\right)^2 - d\Gamma\frac{\partial^4\Gamma}{\partial x^4} + 4d\frac{\partial\Gamma}{\partial x}\frac{\partial^3\Gamma}{\partial x^3} - 3d\left(\frac{\partial^2\Gamma}{\partial x^2}\right)^2 + \Gamma\frac{\partial^2\Gamma}{\partial t^2} - \left(\frac{\partial\Gamma}{\partial t}\right)^2 = 0. \tag{15}$$

3 Results

Next we will consider various types of forms for the function Γ and substitute them in Eq. (15). Then, we expand, evaluate, collect similar terms, and set them equal to 0. Finally, we solve this system of equations to obtain a number of potential sets of solutions for each case.

3.1 Interaction *via* double exponents integral equation (IE)

Following the results in the study by Ceesay *et al.* [57], this wave structure is derived by letting

$$\Gamma(x, t) = h_1 \exp(l(r_1(\lambda t + x) + r_2)) + h_2 \exp(l(r_3(\lambda t + x) + r_4)), \tag{16}$$

where r_i (for $1 \le i \le 4$), h_j (for $1 \le j \le 2$), and $l \ne 0$ are arbitrary constants, and the parameter $\lambda \ne 0$ is the wave speed. Eq. (16) and its first four partial derivatives were substituted in Eq. (15). Then, we reduce the terms algebraically in order to obtain a simplified expression. Assembling similar terms together and equating each expression's coefficient to zero, the following set of constant values resulted:

Set 1. $r_3 = \frac{dl^2 r_1 - \sqrt{d\lambda^2 l^2 - a^2 dl^2}}{dl^2}$.

Substituting this constant in Eq. (16) and the outcome in Eq. (12), we obtain

$$L_{1\mathrm{IE}}(x,t) = \frac{12\left(\frac{h_1\sqrt{dl^2(\lambda^2-a^2)}\,e^{l(r_1(\lambda t+x)+r_2)}}{h_2\exp\left(l\left(-\frac{(\lambda t+x)\sqrt{dl^2(\lambda^2-a^2)}}{dl^2}+r_1(\lambda t+x)+r_4\right)\right)+h_1e^{l(r_1(\lambda t+x)+r_2)}}-\sqrt{dl^2(\lambda^2-a^2)}+dl^2r_1\right)}{bl}, \tag{17}$$

where $a, b, d \neq 0$ are free parameters. Figure 1(a) depicts the solution $L_{1IE}(x,t)$ corresponding to Eq. (17) for selected parameter values $r_1 = 2.2$, $r_2 = 1.2$, $r_4 = 1.6$, $h_1 = 2.4$, $h_2 = 1.4$, $a = 0.4$, $b = 0.62$, $d = 0.5$, $l = 3.9$, $\lambda = 0.34$. Figure 1(b) shows the contour of Figure 1(a).

3.2 Interaction of M-shaped rational wave with one kink (M1K)

This wave configuration is provided by using [58]

$$\Gamma(x,t) = h_1\exp(r_1(\lambda t+x)+r_2) + (r_3(\lambda t+x)+r_4)^2 + (r_5(\lambda t+x)+r_6)^2 + r_7, \tag{18}$$

where r_i (for $1 \le i \le 7$), and h_1 are arbitrary constants, and the parameter $\lambda \neq 0$ is the wave speed. Let us substitute Eq. (18) and its partial derivatives up to the fourth order in Eq. (15) and simplify algebraically. Proceeding as in the previous Section 3.1, we obtain one set of constant values from the resulting system.

Set 1. $r_1 = -\frac{\sqrt{\lambda^2-a^2}}{\sqrt{d}}$, $r_3 = 0$, $r_5 = 0$.

Substituting these values in Eq. (18), and then the resulting equation in Eq. (12), we obtain

$$L_{1\mathrm{M1K}}(x,t) = -\frac{12\sqrt{d}\,h_1e^{r_2}\sqrt{\lambda^2-a^2}}{b(r_4^2+r_6^2+r_7)e^{\frac{\sqrt{\lambda^2-a^2}(\lambda t+x)}{\sqrt{d}}}+bh_1e^{r_2}}, \tag{19}$$

where $a, b, d \neq 0$ are free parameters. The solution $L_{1M1K}(x,t)$ corresponding to Eq. (19) is shown in Figure 2(a) for the parameter values $r_2 = 3.2$, $r_4 = 0.5$, $r_6 = 0.1$, $r_7 = 2.3$, $h_1 = 4.1$, $a = 0.5$, $b = 0.68$, $d = 0.7$, $\lambda = 0.18$. Meanwhile, Figure 2(b) shows its corresponding contour plot.

3.3 Interaction of M-shaped rational wave with two kinks (M2K)

This wave configuration is provided by [58]

$$\Gamma(x,t) = h_1\exp(r_1(\lambda t+x)+r_2) + h_2\exp(r_3(\lambda t+x)+r_4) + (r_5(\lambda t+x)+r_6)^2 + (r_7(\lambda t+x)+r_8)^2 + r_9, \tag{20}$$

where r_i (for $1 \le i \le 9$) and h_j (for $1 \le j \le 2$) are arbitrary constants, and the parameter $\lambda \neq 0$ is the wave speed. Substitute Eq. (20) and its partial derivatives up to the fourth order in Eq. (15) and simplify. Proceeding as before, we obtain a set of constant values.

Set 1. $r_1 = -\frac{\sqrt{\lambda^2-a^2}}{\sqrt{d}}$, $r_3 = -\frac{\sqrt{\lambda^2-a^2}}{\sqrt{d}}$, $r_5 = 0$, $r_7 = 0$, $r_8 = 0$.

After inserting these values in Eq. (20) and the outcome in Eq. (12), we readily obtain

$$L_{1\mathrm{M2K}}(x,t) = -\frac{12\sqrt{d}\sqrt{\lambda^2-a^2}(h_1e^{r_2}+h_2e^{r_4})}{b\left((r_6^2+r_9)e^{\frac{\sqrt{\lambda^2-a^2}(\lambda t+x)}{\sqrt{d}}}+h_1e^{r_2}+h_2e^{r_4}\right)}, \tag{21}$$

where $a, b, d \neq 0$ are free parameters. Figure 3(a) depicts the solution $L_{1M2K}(x,t)$ from Eq. (21) with chosen parameter values $r_2 = 2.0$, $r_4 = 4.6$, $r_6 = 7.2$, $r_9 = 3.3$, $h_1 = 0.3$, $h_2 = 1.9$, $a = 0.5$, $b = 1.08$, $d = 0.1$, $\lambda = 0.11$. Figure 3(b) illustrates its corresponding contour plot.

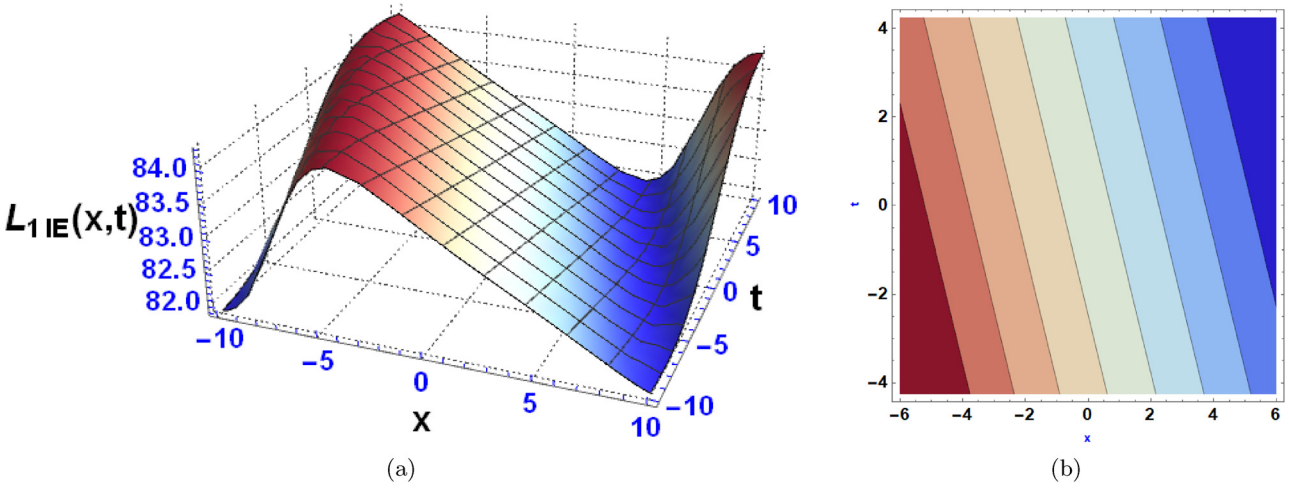

(a) (b)

Figure 1: The three-dimensional (3D) (a) and contour diagram (b) representing the IE-type wave.

3.4 Interaction of multi-lump and periodic solutions (MLP)

This wave configuration is provided by [52]

$$\begin{aligned}\Gamma(x,t) = {} & h_3\sinh(r_1(\lambda t + x) + r_2) + h_4\cosh(r_3(\lambda t + x) + r_4) \\ & + h_1\cos(r_3(\lambda t + x) + r_4)\cosh(r_1(\lambda t + x) + r_2) \\ & + h_2\sin(r_3(\lambda t + x) + r_4)\cosh(r_1(\lambda t \\ & + x) + r_2) + 1,\end{aligned} \tag{22}$$

where r_i (for $1 \le i \le 4$) and h_j (for $1 \le j \le 4$) are arbitrary constants, and the parameter $\lambda \neq 0$ is the wave speed, once again. We substitute Eq. (22) and its first four partial derivatives into Eq. (15), and we simplify algebraically. In similar fashion as with the previous wave structures, we obtain a single set of parameter values.

Set 1. $h_1 = -ih_2$, $h_3 = 0$, $h_4 = 0$, $r_1 = -\frac{\sqrt{\lambda^2 - a^2}}{2\sqrt{d}}$, $r_3 = -\frac{i\sqrt{\lambda^2 - a^2}}{2\sqrt{d}}$.

Substituting these parameter values in Eq. (22) and then the result in Eq. (12), we obtain

$$L_{1\mathrm{MLP}}(x,t) = \frac{6\sqrt{d}\,h_2\sqrt{\lambda^2 - a^2}\left(\sinh\left(\frac{\sqrt{\lambda^2 - a^2}(\lambda t + x)}{\sqrt{d}} - r_2 + ir_4\right) + \cosh\left(\frac{\sqrt{\lambda^2 - a^2}(\lambda t + x)}{\sqrt{d}} - r_2 + ir_4\right)\right)}{b\left(h_2\cosh\left(\frac{\sqrt{\lambda^2 - a^2}(\lambda t + x)}{2\sqrt{d}} - r_2\right)\left(\sinh\left(\frac{\sqrt{\lambda^2 - a^2}(\lambda t + x)}{2\sqrt{d}} + ir_4\right) + \cosh\left(\frac{\sqrt{\lambda^2 - a^2}(\lambda t + x)}{2\sqrt{d}} + ir_4\right)\right) + i\right)}, \tag{23}$$

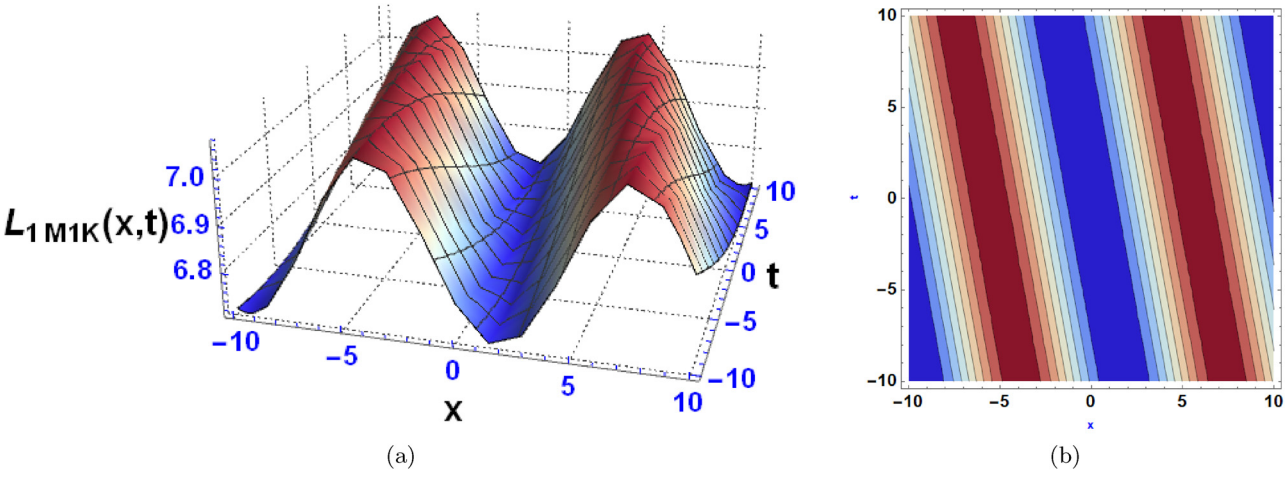

(a) (b)

Figure 2: The 3D (a) and contour diagram (b) of M1K wave-type.

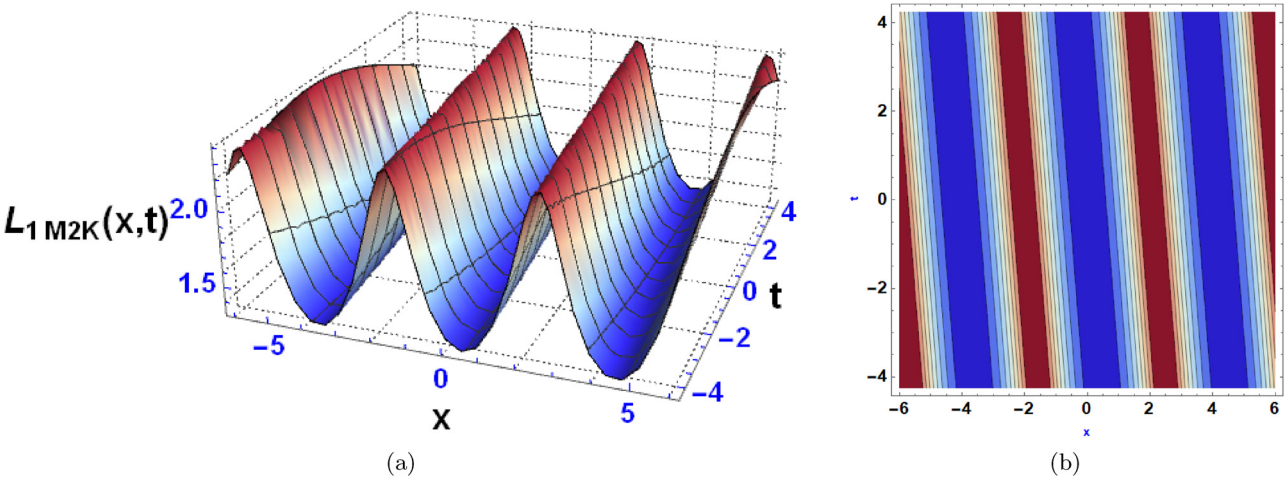

(a) (b)

Figure 3: The 3D (a) and contour diagram (b) of M2K wave-type.

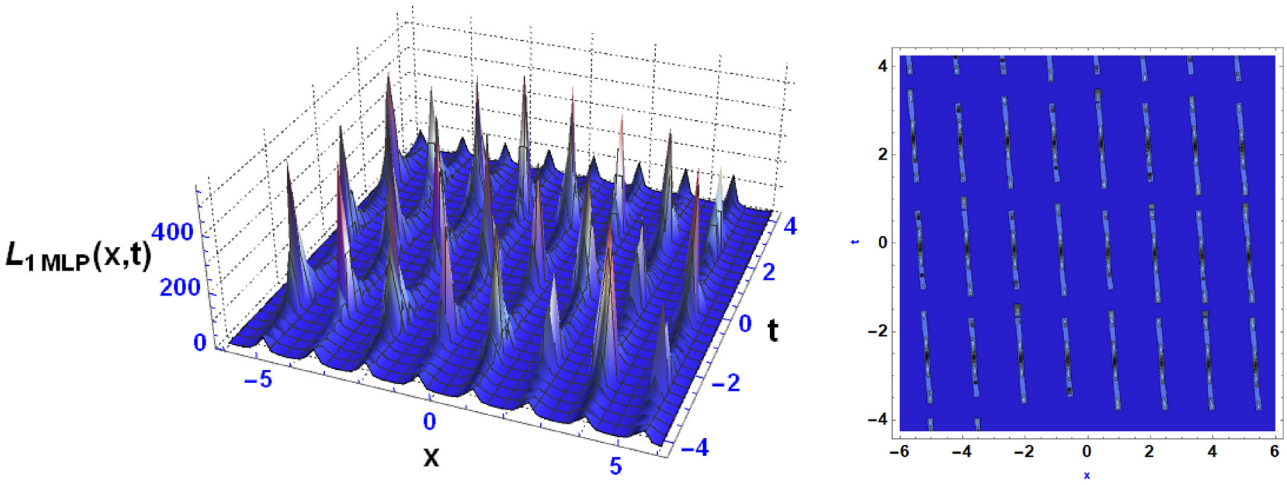

(a) (b)

Figure 4: The 3D (a) and contour diagram (b) are obtained from the MLP wave-type.

where $a, b, d \neq 0$ are free real parameters. Figure 4(a) is obtained from the solution $L_{1\text{MLP}}(x, t)$, corresponding to Eq. (23) for the parameter values $r_2 = 0.2$, $r_4 = 4.0$, $h_2 = 3.1$, $a = 2.3$, $b = 0.82$, $d = 0.3$, $\Lambda = 0.087$. Figure 4(b) represents its respective contour plot.

3.5 Multi waves (MU)

This pattern of waves is derived when [59]

$$\Gamma(x,t) = h_2 \cos(r_3(\lambda t + x) + r_4) + h_1 \cosh(r_1(\lambda t + x) + r_2) + h_3 \cosh(r_5(\lambda t + x) + r_6), \tag{24}$$

where r_i (for $1 \leq i \leq 6$) and h_j (for $1 \leq j \leq 3$) are arbitrary constants, and $\lambda \neq 0$ is the wave speed. Let us substitute Eq. (24) and its first four partial derivatives in Eq. (15), and then we reduce algebraically. Proceeding as in the previous Section 3.4, we obtain two sets of parameter values.

Set 1. $r_1 = \frac{\sqrt{\lambda^2 - a^2}}{2\sqrt{d}}$, $r_3 = \frac{i\sqrt{\lambda^2 - a^2}}{2\sqrt{d}}$, $r_5 = \frac{\sqrt{\lambda^2 - a^2}}{2\sqrt{d}}$.

Substituting them in Eq. (24), and then the result in Eq. (12), yields the solution

$$L_{1\text{MU}}(x,t) = \frac{6\sqrt{d}\sqrt{\lambda^2 - a^2}(h_1 \sinh(A_1 + r_2) + h_2 \sinh(A_1 - ir_4) + h_3 \sinh(A_1 + r_6))}{b(h_1 \cosh(A_1 + r_2) + h_2 \cosh(A_1 - ir_4) + h_3 \cosh(A_1 + r_6))}, \tag{25}$$

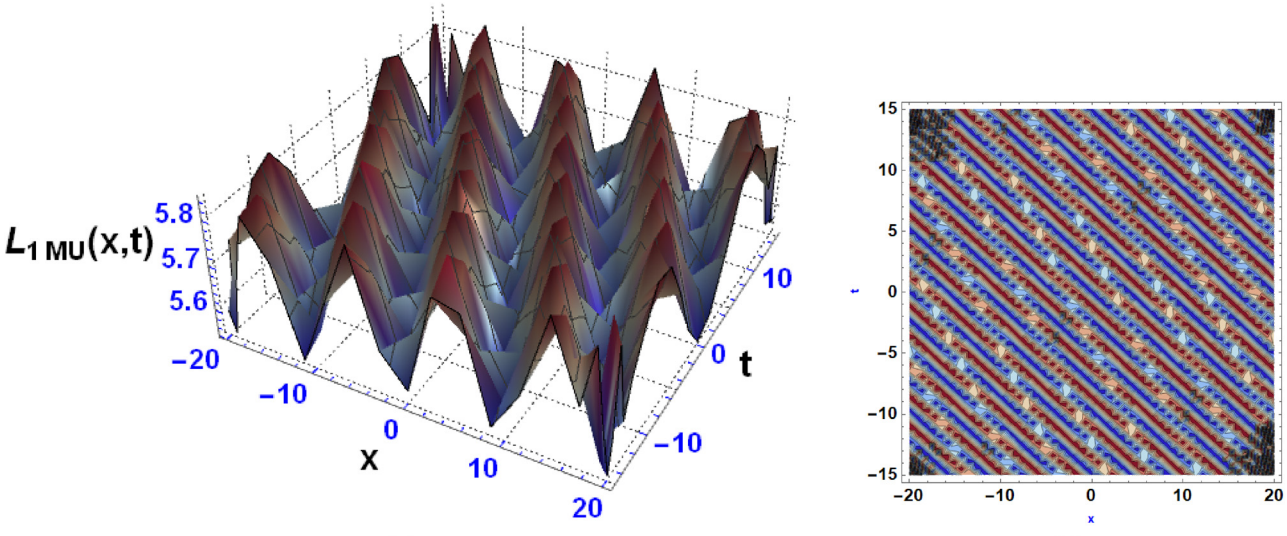

(a) (b)

Figure 5: The 3D (a) and contour diagram (b) of MU wave-type.

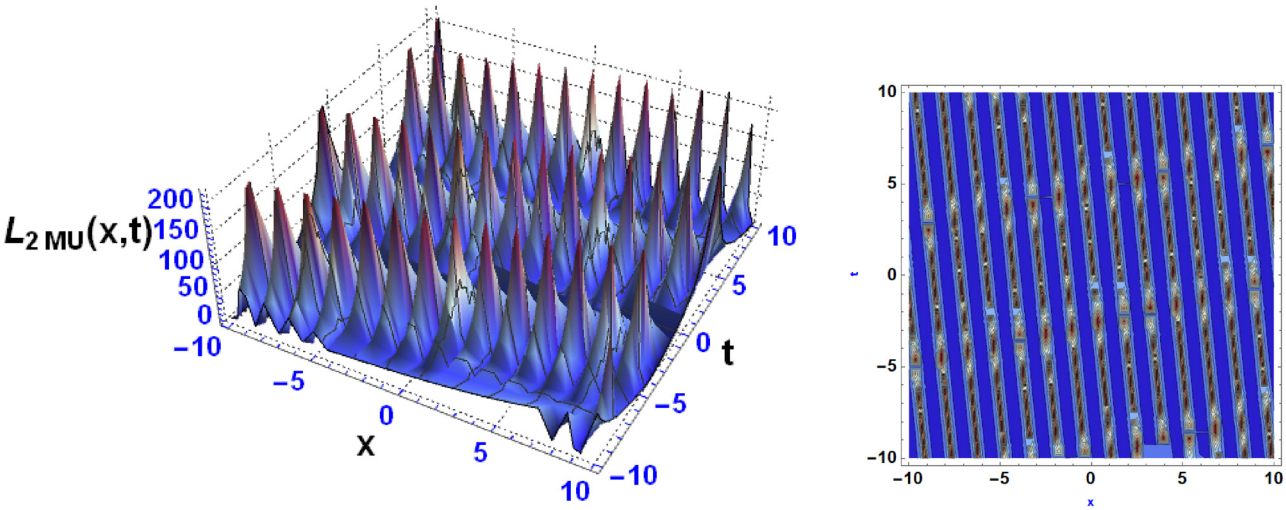

(a) (b)

Figure 6: The 3D (a) and contour diagram (b) of MU wave-type.

where $A_1 = \frac{\sqrt{\lambda^2 - a^2}(\lambda t + x)}{2\sqrt{d}}$, and $a, b, d \neq 0$ are free parameters. Using the solution $L_{1\mathrm{MU}}(x, t)$ from Eq. (25), Figure 5(a) is obtained by selecting the parameter values $r_2 = 2.3$, $r_4 = 5.2$, $r_6 = 2.1$, $h_1 = 6.9$, $h_2 = 0.2$, $h_3 = 9.1$, $a = 4.9$, $b = 2.28$, $d = 0.3$, $\lambda = 2.9$. The associated contour plot is portrayed as Figure 5(b).

Set 2. $h_3 = 0$, $r_1 = \frac{\sqrt{\lambda^2 - a^2}}{2\sqrt{d}}$, $r_3 = \frac{i\sqrt{\lambda^2 - a^2}}{2\sqrt{d}}$.

Substituting them in Eq. (24) and then the result in Eq. (12), we obtain

$$L_{2\mathrm{MU}}(x, t) = \frac{6\sqrt{d}\sqrt{\lambda^2 - a^2}\left(h_1 \sinh\left(\frac{\sqrt{\lambda^2 - a^2}(\lambda t + x)}{2\sqrt{d}} + r_2\right) + h_2 \sinh\left(\frac{\sqrt{\lambda^2 - a^2}(\lambda t + x)}{2\sqrt{d}} - ir_4\right)\right)}{b\left(h_1 \cosh\left(\frac{\sqrt{\lambda^2 - a^2}(\lambda t + x)}{2\sqrt{d}} + r_2\right) + h_2 \cosh\left(\frac{\sqrt{\lambda^2 - a^2}(\lambda t + x)}{2\sqrt{d}} - ir_4\right)\right)}, \tag{26}$$

where $a, b, d \neq 0$ are free parameters. The solution $L_{2\mathrm{MU}}(x, t)$ given by Eq. (26) is represented in Figure 6(a) by selecting the parameter values $r_2 = 0.9$, $r_4 = 2.4$, $h_1 = 1.2$, $h_2 = 3.2$, $a = 3.6$, $b = 0.67$, $d = 0.7$, $\lambda = 0.1$. The corresponding contour plot is shown in Figure 6(b).

3.6 Periodic lump (PL)

This wave structure is given by [59]

$$\Gamma(x, t) = (r_1(\lambda t + x) + r_2)^2 + (r_3(\lambda t + x) + r_4)^2 + \cos(r_5(\lambda t + x) + r_6) + r_7, \tag{27}$$

where r_i (for $1 \leq i \leq 7$) are arbitrary constants, and the parameter $\lambda \neq 0$ is, as usual, the wave speed. Substituting Eq. (27) and its partial derivatives in Eq. (15), and proceeding then as before, we obtain a single set of parameter values.

Set 1. $r_1 = -ir_3$, $r_2 = 0$, $r_4 = 0$, $r_5 = \frac{i\sqrt{\lambda^2 - a^2}}{2\sqrt{d}}$, $r_7 = 0$.

By replacing these parameter values in Eq. (27), and the outcome in Eq. (12), we obtain

$$L_{1\mathrm{PL}}(x, t) = \frac{6\sqrt{d}\sqrt{\lambda^2 - a^2}\tanh\left(\frac{\sqrt{\lambda^2 - a^2}(\lambda t + x)}{2\sqrt{d}} - ir_6\right)}{b}, \tag{28}$$

where $a, b, d \neq 0$ are free parameters. The solution $L_{1\mathrm{LP}}(x, t)$ corresponding to Eq. (28) is depicted in Figure 7(a) with the chosen parameter values $r_6 = 1.2$, $a = 3.77$, $b = 0.47$, $d = 4.8$, $\lambda = 7.41$. Figure 7(b) portrays its corresponding contour.

3.7 Periodic cross kink (PCK)

This type of solution is obtained when [59]

$$\begin{aligned}\Gamma(x, t) = {} & h_1 \exp(l(r_3(\lambda t + x) + r_4)) \\ & + \exp(-l(r_1(\lambda t + x) + r_2)) \\ & + h_2 \cos(l(r_5(\lambda t + x) + r_6)) \\ & + h_3 \cosh(l(r_7(\lambda t + x) + r_8)) + r_9,\end{aligned} \tag{29}$$

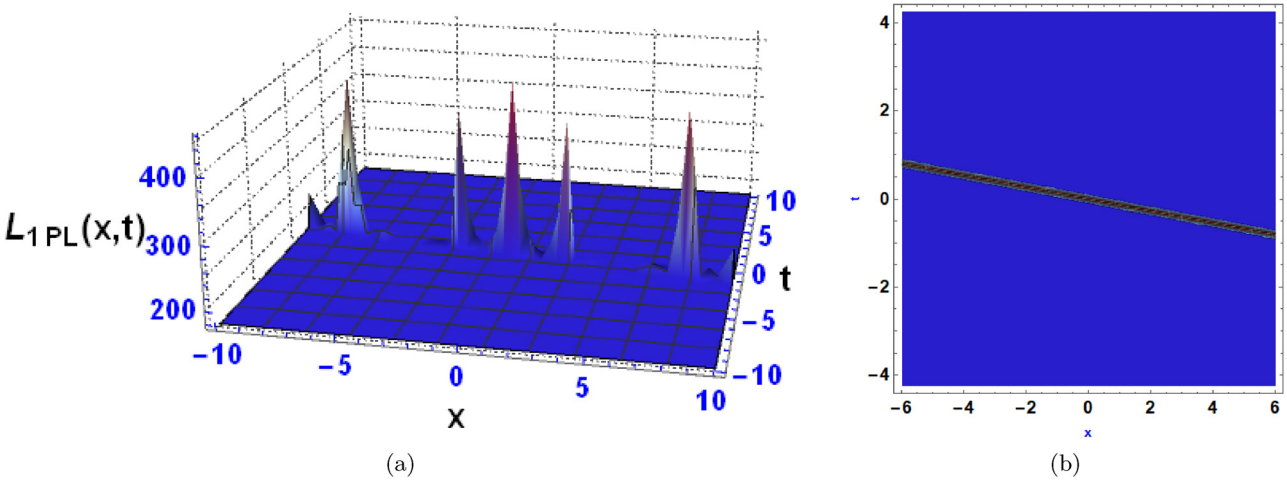

Figure 7: The 3D (a) and contour diagram (b) obtained from PL type wave.

where r_i (for $1 \le i \le 9$), h_j (for $1 \le j \le 3$), and $l \neq 0$ are arbitrary constants, and the parameter $\lambda \neq 0$ is the wave speed. Substitute Eq. (29) and its first four partial derivatives in Eq. (15). Simplifying algebraically and proceeding as previously, we derive two sets of parameter values in this case.

Set 1. $r_1 = -\frac{\sqrt{\lambda^2 - a^2}}{2\sqrt{d}\,l}$, $r_3 = \frac{\sqrt{\lambda^2 - a^2}}{2\sqrt{d}\,l}$, $r_5 = \frac{i\sqrt{\lambda^2 - a^2}}{2\sqrt{d}\,l}$, $r_7 = -\frac{\sqrt{\lambda^2 - a^2}}{2\sqrt{d}\,l}$, $r_9 = 0$.

Inserting them in Eq. (29) and then the outcome in Eq. (12), we have

$$A_2 = h_3 \sinh\left(\frac{\sqrt{\lambda^2 - a^2}(\lambda t + x)}{2\sqrt{d}} - l r_8\right) - i h_2 \sin\left(l\left(r_6 + \frac{i\sqrt{\lambda^2 - a^2}(\lambda t + x)}{2\sqrt{d}\,l}\right)\right), \tag{31}$$

$$A_3 = h_3 \cosh\left(\frac{\sqrt{\lambda^2 - a^2}(\lambda t + x)}{2\sqrt{d}} - l r_8\right) + h_2 \cosh\left(\frac{\sqrt{\lambda^2 - a^2}(\lambda t + x)}{2\sqrt{d}} - i l r_6\right), \tag{32}$$

$$L_{1\mathrm{PCK}}(x,t) = \frac{6\sqrt{d}\sqrt{\lambda^2 - a^2}\left(h_1 \exp\left(\frac{\sqrt{\lambda^2 - a^2}(\lambda t + x)}{2\sqrt{d}} + l(r_2 + r_4)\right) + e^{\frac{\sqrt{\lambda^2 - a^2}(\lambda t + x)}{2\sqrt{d}}} + A_2 e^{l r_2}\right)}{b\left(h_1 \exp\left(\frac{\sqrt{\lambda^2 - a^2}(\lambda t + x)}{2\sqrt{d}} + l(r_2 + r_4)\right) + e^{\frac{\sqrt{\lambda^2 - a^2}(\lambda t + x)}{2\sqrt{d}}} + A_3 e^{l r_2}\right)}, \tag{30}$$

where

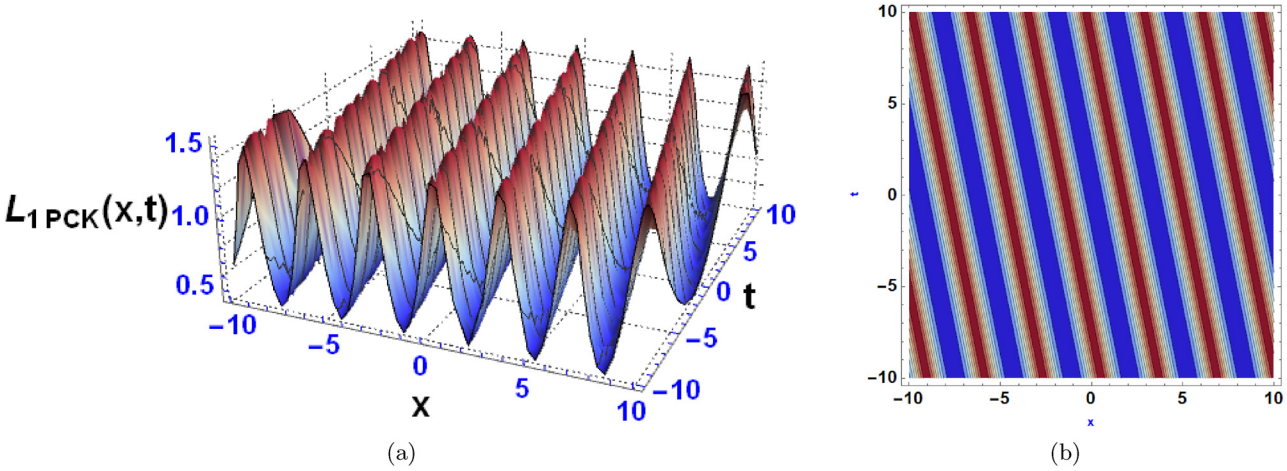

Figure 8: The 3D (a) and contour diagram (b) representing the PCK-type wave.

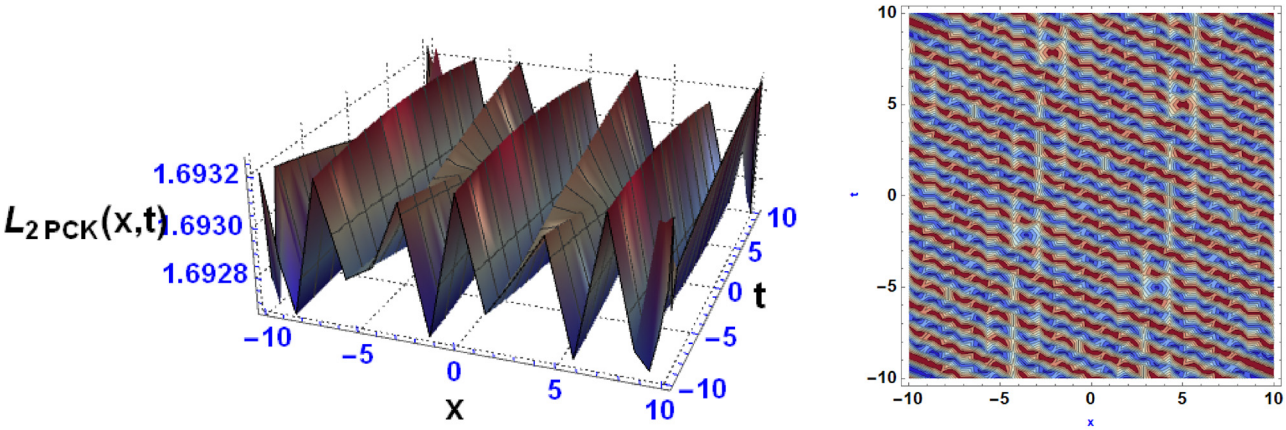

Figure 9: The 3D (a) and contour diagram (b) representing the PCK-type wave.

and $a, b, d \neq 0$ are free parameters. Using the solution $L_{1PCK}(x, t)$ from Eq. (30), Figure 8(a) is obtained by selecting the parameter values $r_2 = 2.3$, $r_4 = 1.8$, $r_6 = 3.1$, $r_8 = 3.1$, $h_1 = 7.1$, $h_2 = 9.4$, $h_3 = 1.7$, $a = 1.1$, $b = 4.32$, $d = 0.3$, $l = 0.9$, $\lambda = 0.2$. As expected, its corresponding contour plot is shown in Figure 8(b).

Set 2. $h_1 = 0$, $r_1 = \frac{\sqrt{\lambda^2 - a^2}}{2\sqrt{d}l}$, $r_5 = \frac{i\sqrt{\lambda^2 - a^2}}{2\sqrt{d}l}$, $r_7 = \frac{\sqrt{\lambda^2 - a^2}}{2\sqrt{d}l}$, $r_9 = 0$.

Plugging these parameter values in Eq. (29) and then the result in Eq. (12), we readily reach

$$L_{2\text{PCK}}(x, t) = \frac{6\sqrt{d}\sqrt{\lambda^2 - a^2}\left(A_2 - e^{-\frac{\sqrt{\lambda^2-a^2}(\lambda t+x)}{2\sqrt{d}} - lr_2}\right)}{b\left(e^{-\frac{\sqrt{\lambda^2-a^2}(\lambda t+x)}{2\sqrt{d}} - lr_2} + A_3\right)}. \quad (33)$$

The solution $L_{2\text{PCK}}(x, t)$ corresponding to Eq. (33) is represented in Figure 9(a) for the parameter values $r_2 = 6.3$, $r_6 = 1.4$, $r_8 = 4.8$, $h_2 = 9.1$, $h_3 = 4.3$, $a = 2.8$, $b = 3.16$, $d = 0.5$, $l = 2.1$, $\lambda = 2.5$. The corresponding contour plot is depicted in Figure 9(b).

3.8 Interactions of exponential, trigonometric, and tanh (ETH)

This wave structure is given by [60]

$$\begin{aligned}\Gamma(x, t) = {} & h_1 \exp(r_1(\lambda t + x) + r_2) \\ & + h_2 \exp(-(r_1(\lambda t + x) + r_2)) \\ & + h_3 \sin(r_3(\lambda t + x) + r_4) \\ & + h_4 \cos(r_5(\lambda t + x) + r_6) \\ & + h_5 \tanh(r_7(\lambda t + x) + r_8),\end{aligned} \quad (34)$$

where r_i (for $1 \leq i \leq 8$) and h_j (for $1 \leq j \leq 5$) are arbitrary constants, and the parameter $\lambda \neq 0$ is the wave speed. Substitute Eq. (34) and its first four partial derivatives in Eq. (15), and proceed as before. In this case, we derive a single set of parameter values.

Set 1. $h_2 = 0$, $r_3 = \frac{\sqrt{a^2 - \lambda^2}}{\sqrt{d}}$, $r_5 = 0$, $r_7 = -\frac{i\sqrt{\lambda^2 - a^2}}{2\sqrt{2}\sqrt{d}}$.

By replacing them in Eq. (34) and the outcome in Eq. (12), we obtain

$$\begin{aligned}&L_{1\text{ETH}}(x, t) \\ &= \frac{3\sqrt{d}\left(4h_3\sqrt{(a-\lambda)(a+\lambda)}\cos\left(\frac{\sqrt{(a-\lambda)(a+\lambda)}(\lambda t+x)}{\sqrt{d}} + r_4\right) - A_4\right)}{b\left(-ih_5\tan\left(\frac{\sqrt{\lambda^2-a^2}(\lambda t+x)}{2\sqrt{2}\sqrt{d}} + ir_8\right) + A_5 + h_4\cos(r_6)\right)},\end{aligned} \quad (35)$$

where

$$\begin{aligned}A_4 = {} & 4\sqrt{d}h_1r_1e^{r_1(\lambda t+x)+r_2} + i\sqrt{2}h_5\sqrt{\lambda^2 - a^2} \\ & \times \sec^2\left(\frac{\sqrt{\lambda^2 - a^2}(\lambda t + x)}{2\sqrt{2}\sqrt{d}} + ir_8\right),\end{aligned} \quad (36)$$

$$\begin{aligned}A_5 = {} & h_3\sin\left(\frac{\sqrt{(a-\lambda)(a+\lambda)}(\lambda t + x)}{\sqrt{d}} + r_4\right) \\ & + h_1e^{r_1(\lambda t+x)+r_2},\end{aligned} \quad (37)$$

and $a, b, d \neq 0$ are free parameters. The solution $L_{1\text{ETH}}(x, t)$ given by Eq. (35) is shown in Figure 10(a) for the parameter values $r_1 = 2.3$, $r_2 = 2.3$, $r_4 = 1.8$, $r_6 = 3.1$, $r_8 = 3.1$, $h_1 = 7.1$, $h_3 = 9.4$, $h_4 = 1.7$, $h_5 = 1.7$, $a = 1.1$, $b = 4.32$, $d = 0.3$, $\lambda = 5.2$. Figure 10(b) shows the related contour plot.

3.9 Mixed waves (MI)

This pattern of waves is derived by letting [61]

$$\begin{aligned}\Gamma(x,t) &= h_1\exp(l(r_1(\lambda t+x)+r_2))\\ &+ h_2\exp(-l(r_1(\lambda t+x)+r_2))\\ &+ h_3\sin(l(r_3(\lambda t+x)+r_4))\\ &+ h_4\sinh(l(r_5(\lambda t+x)+r_6)),\end{aligned} \tag{38}$$

where r_i (for $1 \le i \le 6$), h_j (for $1 \le j \le 4$), and $l \neq 0$ are arbitrary constants, and the parameter $\lambda \neq 0$ is the wave speed. Proceeding as before, we obtain two sets of parameter values in this case.

Set 1. $r_1 = \frac{\sqrt{\lambda^2-a^2}}{2\sqrt{d}\,l}$, $r_3 = \frac{i\sqrt{\lambda^2-a^2}}{2\sqrt{d}\,l}$, $r_5 = \frac{\sqrt{\lambda^2-a^2}}{2\sqrt{d}\,l}$.

In this case, we derive the solution

$$L_{1\mathrm{MI}}(x,t) = \frac{6\sqrt{d}\sqrt{\lambda^2-a^2}\left(A_6 e^{\frac{\sqrt{\lambda^2-a^2}(\lambda t+x)}{2\sqrt{d}}+lr_2} + h_1 e^{\frac{\sqrt{\lambda^2-a^2}(\lambda t+x)}{\sqrt{d}}+2lr_2} - h_2\right)}{b\left(A_7 e^{\frac{\sqrt{\lambda^2-a^2}(\lambda t+x)}{2\sqrt{d}}+lr_2} + h_1 e^{\frac{\sqrt{\lambda^2-a^2}(\lambda t+x)}{\sqrt{d}}+2lr_2} + h_2\right)}, \tag{39}$$

where

$$\begin{aligned}A_6 &= h_4\cosh\left(\frac{\sqrt{\lambda^2-a^2}(\lambda t+x)}{2\sqrt{d}} + lr_6\right)\\ &+ ih_3\cosh\left(\frac{\sqrt{\lambda^2-a^2}(\lambda t+x)}{2\sqrt{d}} - ilr_4\right),\end{aligned} \tag{40}$$

$$\begin{aligned}A_7 &= h_4\sinh\left(\frac{\sqrt{\lambda^2-a^2}(\lambda t+x)}{2\sqrt{d}} + lr_6\right)\\ &+ h_3\sin\left(l\left(r_4 + \frac{i\sqrt{\lambda^2-a^2}(\lambda t+x)}{2\sqrt{d}\,l}\right)\right),\end{aligned} \tag{41}$$

and $a, b, d \neq 0$ are free parameters. The solution $L_{1\mathrm{MI}}(x,t)$ given by Eq. (39) is depicted in Figure 11(a) by selecting the parameter values $r_2 = 7.7$, $r_4 = 1.8$, $r_6 = 3.1$, $h_1 = 7.1$, $h_2 = 9.4$, $h_3 = 1.7$, $h_4 = 4.5$, $a = 2.1$, $b = 1.26$, $d = 1.3$, $l = 0.9$, $\lambda = 0.8$. In turn, Figure 11(b) shows the corresponding contour plot.

Set 2. $h_2 = 0$, $r_1 = \frac{\sqrt{\lambda^2-a^2}}{2\sqrt{d}\,l}$, $r_3 = \frac{i\sqrt{\lambda^2-a^2}}{2\sqrt{d}\,l}$, $r_5 = -\frac{\sqrt{\lambda^2-a^2}}{2\sqrt{d}\,l}$.

In this case, we obtain the solution

$$L_{2\mathrm{MI}}(x,t) = \frac{6\sqrt{d}\sqrt{\lambda^2-a^2}\left(A_8 - h_4\cosh\left(\frac{\sqrt{\lambda^2-a^2}(\lambda t+x)}{2\sqrt{d}} - lr_6\right)\right)}{b\left(A_9 - h_4\sinh\left(\frac{\sqrt{\lambda^2-a^2}(\lambda t+x)}{2\sqrt{d}} - lr_6\right)\right)}, \tag{42}$$

where

$$\begin{aligned}A_8 &= h_1 e^{\frac{\sqrt{\lambda^2-a^2}(\lambda t+x)}{2\sqrt{d}}+lr_2}\\ &+ ih_3\cosh\left(\frac{\sqrt{\lambda^2-a^2}(\lambda t+x)}{2\sqrt{d}} - ilr_4\right),\end{aligned} \tag{43}$$

$$\begin{aligned}A_9 &= h_1 e^{\frac{\sqrt{\lambda^2-a^2}(\lambda t+x)}{2\sqrt{d}}+lr_2}\\ &+ h_3\sin\left(l\left(r_4 + \frac{i\sqrt{\lambda^2-a^2}(\lambda t+x)}{2\sqrt{d}\,l}\right)\right),\end{aligned} \tag{44}$$

and $a, b, d \neq 0$ are free parameters. The solution $L_{1\mathrm{MI}}(x,t)$ corresponding to Eq. (42) is shown in Figure 12(a) for the parameter values $r_2 = 1.4$, $r_4 = 0.6$, $r_6 = 4.6$, $h_1 = 4.8$, $h_3 = 5.7$, $h_4 = 7.8$, $a = 8.4$, $b = 2.83$, $d = 4.2$, $l = 3.1$, $\lambda = 0.5$. The corresponding contour plot is shown in Figure 12(b).

3.10 Homoclinic breather (HB)

This pattern of waves is reached when [61]

$$\begin{aligned}\Gamma(x,t) &= h_1\exp(l(r_1(\lambda t+x)+r_2))\\ &+ h_2\exp(-l(r_3(\lambda t+x)+r_4))\\ &+ h_3\cos(l(r_5(\lambda t+x)+r_6)),\end{aligned} \tag{45}$$

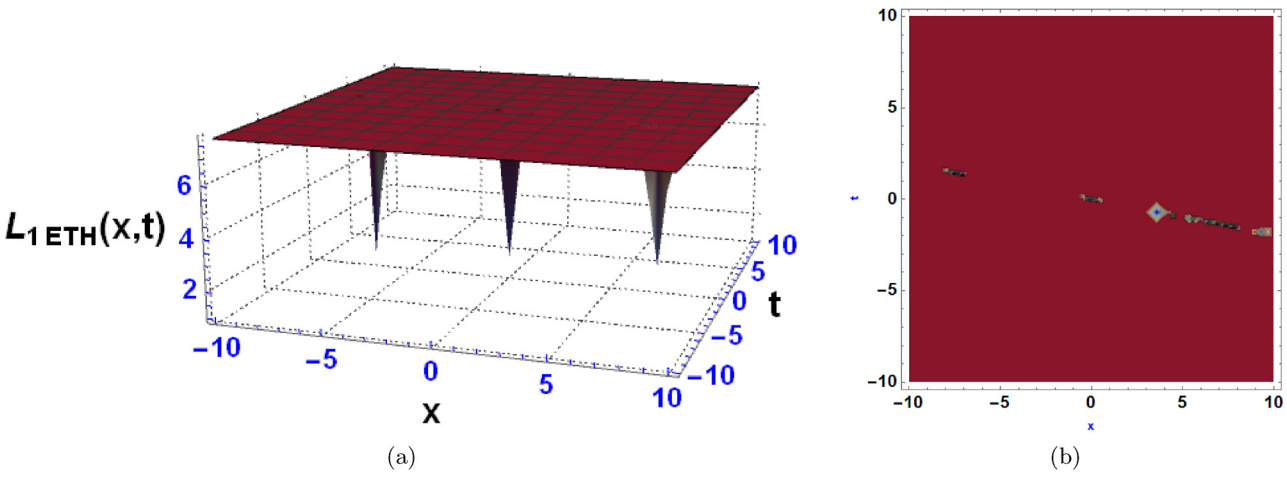

Figure 10: The 3D (a) and contour diagram (b) representing the ETH-type wave.

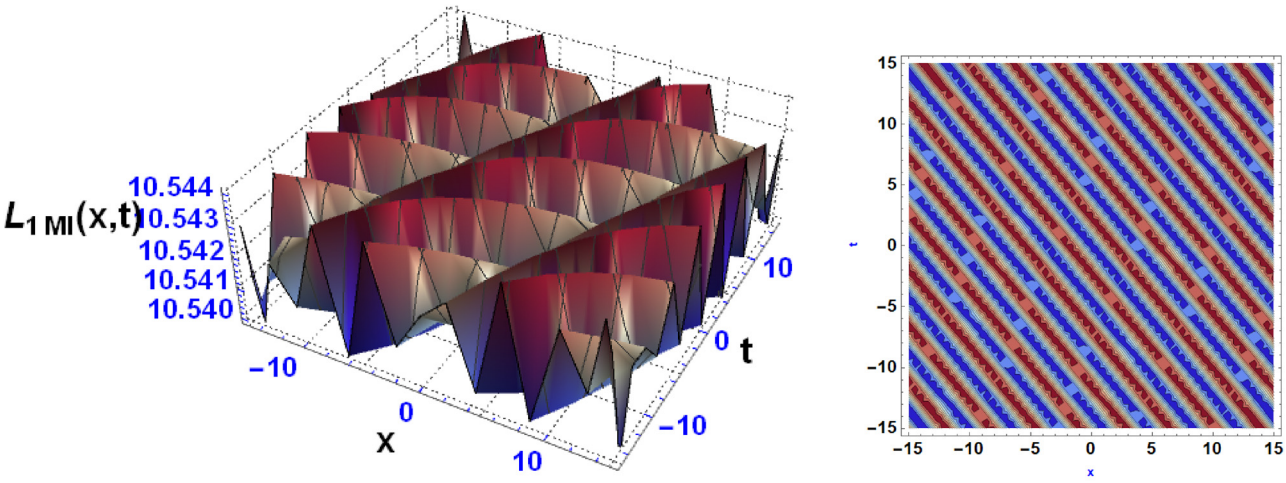

(a) (b)

Figure 11: The 3D (a) and contour diagram (b) representing the MI-type wave.

where r_i (for $1 \le i \le 6$), h_j (for $1 \le j \le 3$), and $l \neq 0$ are arbitrary constants, and the parameter $\lambda \neq 0$ is the wave speed, as usual. Eq. (38) and its first four partial derivatives were substituted in Eq. (15) and we obtain a simplified expression. We collecting similar terms and equated their coefficients to zero, resulting in the following sets of constant values.

Set 1. $r_1 = ir_5$, $r_3 = -ir_5$, $l = \frac{i\sqrt{\lambda^2 - a^2}}{2\sqrt{d}r_5}$.

Inserting them in Eq. (45) and then the outcome in Eq. (12), we obtain

$$L_{1\mathrm{HB}}(x,t) = -\frac{6\sqrt{d}\sqrt{\lambda^2 - a^2}\left(-A_{10}h_3\sinh\left(\frac{\sqrt{\lambda^2 - a^2}(r_5(\lambda t + x) + r_6)}{2\sqrt{d}r_5}\right) + h_1 e^{\frac{i(r_2+r_4)\sqrt{\lambda^2-a^2}}{2\sqrt{d}r_5}} + h_2\right)}{b\left(A_{10}h_3\cosh\left(\frac{\sqrt{\lambda^2 - a^2}(r_5(\lambda t + x) + r_6)}{2\sqrt{d}r_5}\right) + h_1 e^{\frac{i(r_2+r_4)\sqrt{\lambda^2-a^2}}{2\sqrt{d}r_5}} + h_2\right)}, \tag{46}$$

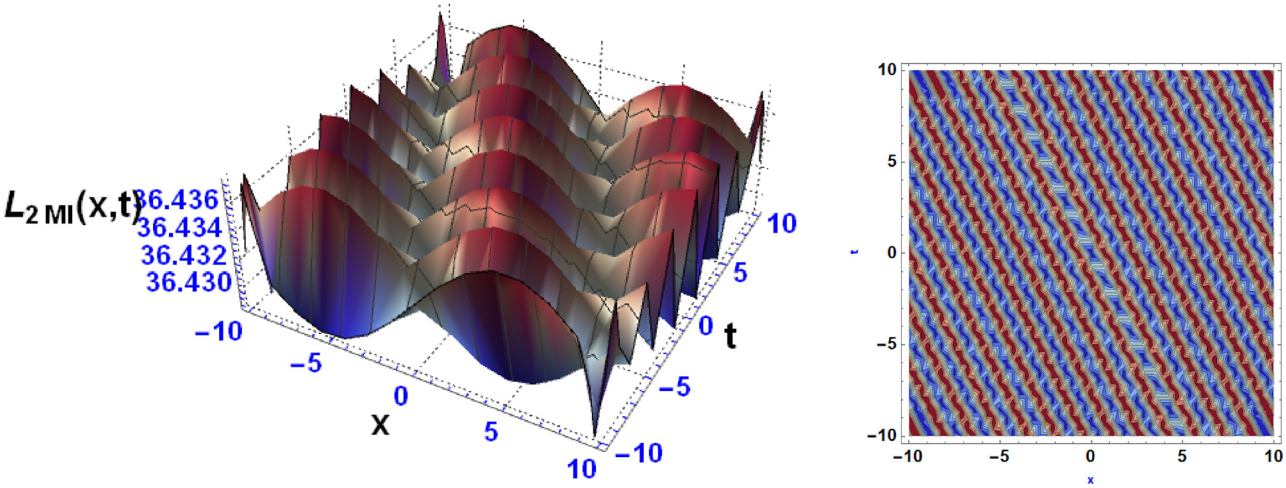

(a) (b)

Figure 12: The 3D (a) and contour diagram (b) representing the MI-type wave.

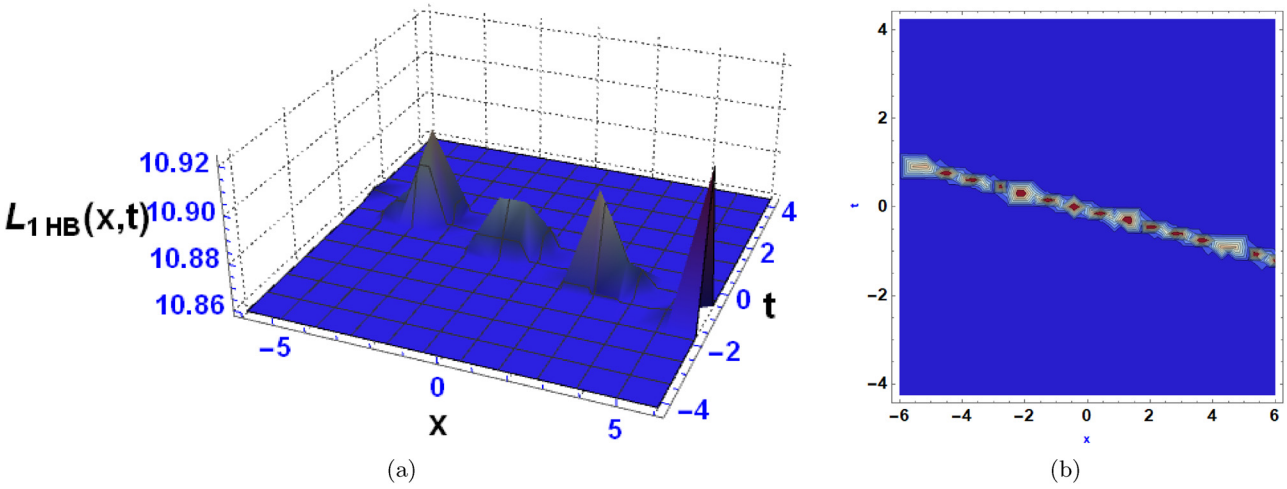

(a) (b)

Figure 13: The 3D (a) and contour diagram (b) representing the HB-type wave.

where

$$A_{10} = \exp\left(\frac{\sqrt{\lambda^2 - a^2}(r_5(\lambda t + x) + ir_4)}{2\sqrt{d}\, r_5}\right), \tag{47}$$

and $a, b, d \neq 0$ are free parameters. Based on the solution $L_{1\mathrm{Hom}}(x, t)$ given by Eq. (46), Figure 13(a) is obtained by selecting the parameter values $r_2 = 9.2$, $r_4 = 0.2$, $r_5 = 0.3$, $r_6 = 0.4$, $h_1 = 3.5$, $h_2 = 1.7$, $h_3 = 3.6$, $a = 2.0$, $b = 3.16$, $d = 1.3$, $\lambda = 5.4$. The corresponding contour plot is given by Figure 13(b).

Set 2. $h_1 = 0$, $r_3 = -ir_5$, $l = \frac{i\sqrt{\lambda^2 - a^2}}{2\sqrt{d}\, r_5}$.

In this case, we derive the exact solution

$$L_{2\mathrm{HB}}(x, t) = -\frac{6\sqrt{d}\sqrt{\lambda^2 - a^2}\left(h_2 - h_3 \exp\left(\frac{\sqrt{\lambda^2 - a^2}(r_5(\lambda t + x) + ir_4)}{2\sqrt{d}\, r_5}\right)\sinh\left(\frac{\sqrt{\lambda^2 - a^2}(r_5(\lambda t + x) + r_6)}{2\sqrt{d}\, r_5}\right)\right)}{b\left(h_2 + h_3 \exp\left(\frac{\sqrt{\lambda^2 - a^2}(r_5(\lambda t + x) + ir_4)}{2\sqrt{d}\, r_5}\right)\cosh\left(\frac{\sqrt{\lambda^2 - a^2}(r_5(\lambda t + x) + r_6)}{2\sqrt{d}\, r_5}\right)\right)}, \tag{48}$$

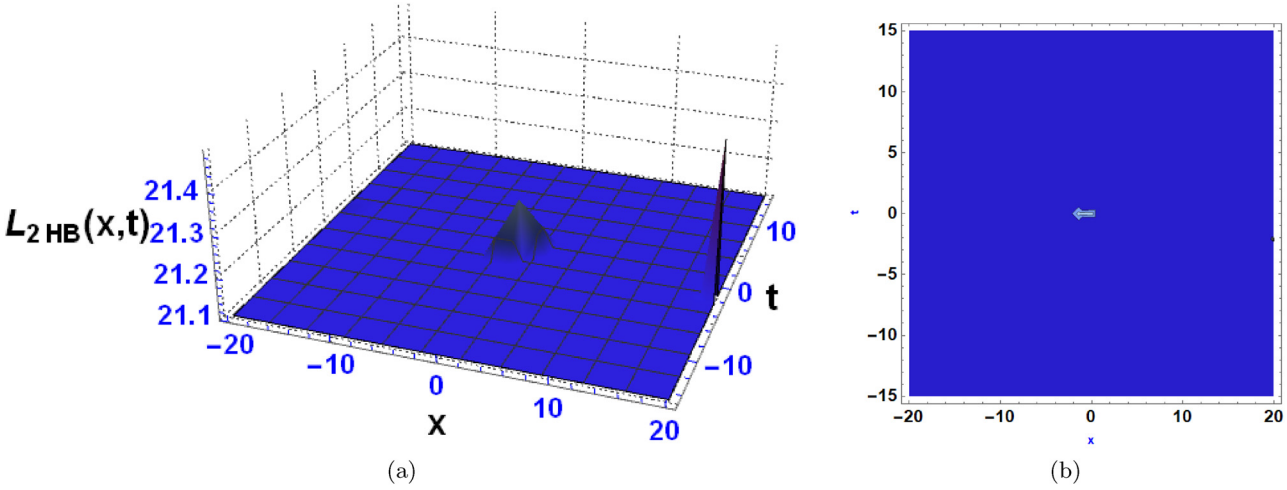

(a) (b)

Figure 14: The 3D (a) and contour diagram (b) representing the HB-type wave.

where $a, b, d \neq 0$ are free parameters. The solution $L_{2\text{Hom}}(x, t)$ given by Eq. (48) is shown in Figure 14(a) for the parameter values $r_4 = 0.2$, $r_5 = 0.3$, $r_6 = 0.4$, $h_2 = 1.7$, $h_3 = 4.2, a = 5.5, b = 3.7, d = 2.5, \lambda = 9.9$. The respective contour plot is given by Figure 14(b).

4 Discussion

Beforehand, it is important to point out that the functions obtained in Section 3 were substituted into the mathematical model using Mathematica software. The results confirm that, indeed, the functions are solutions of our mathematical model. The 3D graphs and their corresponding contour plots for the solutions derived in the previous section were obtained using Mathematica. The graphs are displayed in Figures 1–14 in order to help in visualizing the characteristic of the solutions. Figure 1(a) shows an anti-kink wave obtained from an interaction between two exponential wave functions. Figure 2(a) shows an M-shaped wave with single kink obtained from an interaction between one M-shaped and one kink wave functions. In Figure 3(a), an M-shaped wave with double kinks is portrayed arising from the wave function of M-shaped and two kinks interactions. Figure 4(a) depicts multiple PL waves obtained from the interaction of multi-lump and periodic wave functions. In turn, Figure 5(a) shows a solitary wave derived from a multi wave function, and Figure 6(a) show multiple PL waves obtained from multi wave functions. Figure 7(a) shows periodic bright lump waves obtained from PL wave structures. Figures 8(a) and 9(a) show PCK waves. In Figure 10(a), we have three dark lump strip waves obtained from the interactions of ETH functions. In Figures 11(a) and 12(a), we obtained solitary waves solutions derived from mixed wave functions. In Figure 13(a), we witnessed three bright breather waves from the HB function, whereas in Figure 14(a) we obtained a single layer of bright breather from the same HB wave function. In each case, Figures 1(b) through 14(b) show the corresponding contour plots. These plots assist in the visualization of the wave profiles by displaying changes in both shape and intensity in different spatial areas at different times. Moreover, concrete physical interpretations of these solutions could be provided by scientists in the context of atomic physics.

These wave phenomena obtained from an atomic chain model each represent distinct physical behaviors. The anti-kink wave transitions between two states in a smooth, sharp manner, but the M-shaped wave with a single kink has a peak structure and a sharp transition point, suggesting localized energy concentration. The M-shaped wave with multiple kinks increases complexity with two abrupt transitions, resulting in steeper atomic movement. Periodic multiple lump waves result from multi-lump and periodic wave interactions, with recurrent localized disruptions indicating oscillating energy. Solitary waves travel without changing form and indicate steady energy transmission across the chain, whereas multiple PL waves cause these localized disruptions to repeat on a regular basis. Periodic bright lump waves identify places with significant energy concentration. PCK waves are the outcome of multidimensional kink interactions that generate crossing wave structures. Dark lump strip waves have a lesser intensity resulting in localized amplitude depressions. Solitary wave solutions formed from mixed wave functions exhibit stable, non-dispersive wave forms. Bright breather waves and their single-layer counterparts show localized, periodic energy variations as they surface in and out over time. These waves together demonstrate complicated energy transfer and atomic displacement dynamics in nonlinear atomic systems.

5 Conclusion

This work investigated a diverse spectrum of solitary and soliton solutions resulting from various symmetry wave functions in a nonlinear atomic chain model. The Hirota bilinear transformation approach was used to unveil a wide range of complicated wave phenomena, including anti-kink waves, M-shaped interacting with kink waves, and PL waves. The combination of exponential, trigonometric, and hyperbolic functions has demonstrated its efficiency in revealing various wave forms such as bright breather waves, periodic bright lump waves, and dark lump strip waves, all of which are required to understand localized energy dynamics in these systems. The graphical illustrations, which included 3D and contour plots, contributed to a better understanding of waveform behavior by showing how solitary and periodic wave structures change spatially and temporally. These findings may shed light on the mechanics of energy transfer and atomic displacement in nonlinear atomic chains, highlighting both stability and the possibility for complex wave interactions. Finally, this study not only adds to the theoretical framework of wave dynamics in nonlinear systems, but it also has potential applications in fields like condensed matter physics and material science, where understanding wave interactions in atomic structures is critical for developing new technologies. The discoveries pave the way for further research into more complicated wave phenomena and their

practical consequences in advanced scientific and industrial applications.

As a follow-up to this work, various avenues of research are still open. For instance, the problem of investigating the physical model which considers long-range interactions is an interesting topic of research. In that case, the continuum-limit approximation leads to a fully fractional partial differential equation. In that case, the fractional derivatives appear in the spatial variables. For such system, the derivation of solitary wave solutions and soliton-like solutions is a task that merits attention. In addition, it is worthwhile to point out that the mathematical model studied in the present work is a one-dimensional system in space. This model corresponds to the continuum-limit of a system of particles distributed on a straight line. The case when the atoms are distributed on a plane or inside a three-dimensional volume was not tackled in the present investigation. This is a limitation of our work and, at the same time, a potential direction for future work in the area. Moreover, the elucidation of real-life applications of the results obtained in the present work is also an important problem which needs future attention. Finally, as one of the reviewers pointed out, the exact solutions obtained in this work possess a lot of parameters, and the choice of parameter values to guarantee that a particular solution has a specific wave pattern is certainly a complex task. Such analysis could be the topic of a future report in the context of nonlinear physics.

Acknowledgments: The authors wish to thank the anonymous reviewers and the editor in charge of handling this manuscript for their comments and criticisms. Their suggestions helped in improving substantially the quality of the present report.

Funding information: The authors wish to thank the financial support of the University of Guadalajara, Mexico, through the program PROSNI.

Author contributions: Conceptualization: N.A. and J.E.M.D.; methodology: B.C., M.Z.B., N.A., J.E.M.D., and S.M.; software: B.C., M.Z.B., N.A., J.E.M.D., and S.M.; validation: B.C., M.Z.B., N.A., J.E.M.D., and S.M.; formal analysis: B.C., M.Z.B., N.A., J.E.M.D., and S.M.; investigation: B.C., M.Z.B., N.A., J.E.M.D., and S.M.; resources, B.C., M.Z.B., N.A., J.E.M.D., and S.M.; data curation, B.C., M.Z.B., N.A., J.E.M.D., and S.M.; writing - original draft preparation, B.C., M.Z.B., N.A., J.E.M.D., and S.M.; writing - review and editing: B.C., M.Z.B., N.A., J.E.M.D. and S.M.; visualization: B.C., M.Z.B., N.A., J.E.M.D., and S.M.; supervision: N.A. and J.E.M.D.; project administration: N.A. and J.E.M.D. All authors have accepted responsibility for the entire content of this manuscript and approved its submission.

Conflict of interest: The authors state no conflict of interest.

Data availability statement: All data generated or analysed during this study are included in this published article.

References

[1] Briani M, Denaro CA, Piccoli B, Rarità L. Dynamics of particulate emissions in the presence of autonomous vehicles. Open Math. 2025;23(1):20240126.

[2] Briani M, Manzo R, Piccoli B, Rarità L. Estimation of NOx and O3 reduction by dissipating traffic waves. Netw Heterogeneous Media. 2024;19(2):822–41.

[3] Rarità L. Optimization approaches to manage congestions for the phenomenon “Luci D’Artista” in Salerno. In Proceedings of 32nd European Modeling and Simulation Symposium, EMSS 2020; 2020. p. 319–24.

[4] Alharbi AR, Almatrafi MB, Lotfy K. Constructions of solitary travelling wave solutions for Ito integro-differential equation arising in plasma physics. Results Phys. 2020;19:103533.

[5] Agrawal G. P. Nonlinear fiber optics. In Nonlinear science at the dawn of the 21st century. Berlin, Heidelberg: Springer Berlin Heidelberg; 2000. p. 195–211.

[6] Hafez MG, Kauser MA, Akter MT. Some new exact traveling wave solutions for the Zhiber-Shabat equation. British J Math Comput Sci. 2014;4(18):2582–93.

[7] Singh SS. Solutions of Kudryashov-Sinelshchikov equation and generalized Radhakrishnan-Kundu-Lakshmanan equation by the first integral method. Int J Phys Res. 2016;4(2):37–42.

[8] Rawashdeh M. Using the reduced differential transform method to solve nonlinear PDEs arises in biology and physics. World Appl Sci J. 2013;23(8):1037–43.

[9] Shakeel M, Attaullah, Shah NA, Chung JD. Modified exp-function method to find exact solutions of microtubules nonlinear dynamics models. Symmetry. 2023;15(2):360.

[10] Liu F, Feng Y. The modified generalized Kudryashov method for nonlinear space-time fractional partial differential equations of Schrödinger type. Results Phys. 2023;53:106914.

[11] Chen Y, Wang Q. Extended Jacobi elliptic function rational expansion method and abundant families of Jacobi elliptic function solutions to (1+1)-dimensional dispersive long wave equation. Chaos Solitons Fractals. 2005;24(3):745–57.

[12] Ahmed N, Baber MZ, Iqbal MS, Annum A, Ali SM, Ali M, et al. Analytical study of reaction diffusion Lengyel-Epstein system by generalized Riccati equation mapping method. Sci Rep. 2023;13(1):20033.

[13] Kundu PR, Fahim MRA, Islam ME, Akbar MA. The sine-Gordon expansion method for higher-dimensional NLEEs and parametric analysis. Heliyon. 2021;7(3):e06459.

[14] Wang M, Li X, Zhang J. The $(\frac{G'}{G})$-expansion method and travelling wave solutions of nonlinear evolution equations in mathematical physics. Phys Lett A. 2008;372(4):417–23.
[15] Ozisik M, Secer A, Bayram M. On solitary wave solutions for the extended nonlinear Schrödinger equation via the modified F-expansion method. Opt Quantum Electron. 2023;55(3):215.
[16] Alsharidi A. K., Bekir A. Discovery of new exact wave solutions to the M-fractional complex three coupled Maccari's system by Sardar sub-equation scheme. Symmetry. 2023;15(8):1567.
[17] Ali A, Ahmad J, Javed S. Dynamic investigation to the generalized Yu-Toda-Sasa-Fukuyama equation using Darboux transformation. Opt Quantum Electron. 2024;56(2):166.
[18] Abd-Alhalem SM, Marie HS, El-Shafai W, Altameem T, Rathore RS, Hassan TM. Cervical cancer classification based on a bilinear convolutional neural network approach and random projection. Eng Appl Artif Intel. 2024;127:107261.
[19] Ali N, Zada L, Nawaz R, Jamshed W, Ibrahim RW, Guedri K, Khalifa HAEW. Analysis and simulation of arbitrary order shallow water and Drinfeld-Sokolov-Wilson equations: Natural transform decomposition method. Int J Modern Phys B, 2024;38(6):2450088.
[20] Qing W, Pan B. Modified fractional homotopy method for solving nonlinear optimal control problems. Nonl Dyn. 2024;112(5):3453–79.
[21] Khan M, Hussain M. Application of Laplace decomposition method on semi-infinite domain. Numer Alg. 2011;56:211–8.
[22] Abdelrazec A, Pelinovsky D. Convergence of the Adomian decomposition method for initial-value problems. Numer Meth Partial Differ Equ. 2011;27(4):749–66.
[23] Luke JC. A perturbation method for nonlinear dispersive wave problems. Proc R Soc London Ser A Math Phys Sci. 1966;292(1430):403–12.
[24] Zhang RF, Li MC. Bilinear residual network method for solving the exactly explicit solutions of nonlinear evolution equations. Nonl Dyn. 2022;108(1):521–31.
[25] Kyame JJ. Wave propagation in piezoelectric crystals. J Acoust Soc Am. 1949;21(3):159–67.
[26] Koleshko VM, Meshkov YV, Barkalin VV. Strain effect in single-crystal silicon-based multilayer surface acoustic wave structures. Thin Solid Films. 1990;190(2):359–72.
[27] Priyadarshan P, Rikendra RK. Analysis of wave motion at the solid-solid interface. In: International Conference On Artificial Intelligence Of Things For Smart Societies. Cham: Springer Nature Switzerland; 2024. p. 149–58.
[28] Abbagari S, Houwe A, Akinyemi L, Bouetou TB. Solitonic rogue waves induced by the modulation instability in a split-ring-resonator-based left-handed coplanar waveguide. Chin J Phys 2024;92:1614–27.
[29] Akinyemi L, Manukure S, Houwe A, Abbagari S. A study of (2+1)-dimensional variable coefficients equation: Its oceanic solitons and localized wave solutions. Phys Fluids. 2024;36(1):013120.
[30] Akinyemi L, Houwe A, Abbagari S, Wazwaz AM, Alshehri HM, Osman MS. Effects of the higher-order dispersion on solitary waves and modulation instability in a monomode fiber. Optik. 2023;288:171202.
[31] Mukam SPT, Souleymanou A, Kuetche VK, Bouetou TB. Rogue wave dynamics in barotropic relaxing media. Pramana 2018;91:1–4.
[32] Abbagari S, Youssoufa S, Tchokouansi HT, Kuetche VK, Bouetou TB, Kofane TC. N-rotating loop-soliton solution of the coupled integrable dispersionless equation. J Appl Math Phys. 2017;5(6):1370–9.
[33] Souleymanou A, Kuetche VK, Bouetou TB, Kofane TC. Traveling wave-guide channels of a new coupled integrable dispersionless system. Commun Theoretic Phys. 2012;57(1):10.
[34] Souleymanou A, Kuetche VK, Bouetou TB, Kofane TC. Scattering behavior of waveguide channels of a new coupled integrable dispersionless system. Chin Phys Lett. 2011;28(12):120501.
[35] Seadawy AR, Ahmed HM, Rabie WB, Biswas A. Chirp-free optical solitons in fiber Bragg gratings with dispersive reflectivity having polynomial law of nonlinearity. Optik. 2021;225:165681.
[36] Jhangeer A, Hussain A, Junaid-U-Rehman M, Baleanu D, Riaz MB. Quasi-periodic, chaotic and travelling wave structures of modified Gardner equation. Chaos Solitons Fractals. 2021;143:110578.
[37] Braun OM, Kivshar YS. The Frenkel-Kontorova model: concepts, methods, and applications. Vol. 18. Berlin: Springer; 2004.
[38] Peyrard M, Remoissenet M. Solitonlike excitations in a one-dimensional atomic chain with a nonlinear deformable substrate potential. Phys Rev B. 1982;26(6):2886.
[39] Fang X, Wen J, Yin J, Yu D. Wave propagation in nonlinear metamaterial multi-atomic chains based on homotopy method. AIP Adv. 2016;6(12):121706.
[40] Khater AH, Callebaut DK, Seadawy AR. General soliton solutions for nonlinear dispersive waves in convective type instabilities. Phys Scr. 2006;74(3):384.
[41] Kumar S, Kumar D, Kumar A. Lie symmetry analysis for obtaining the abundant exact solutions, optimal system and dynamics of solitons for a higher-dimensional Fokas equation. Chaos Solitons Fractals. 2021;142:110507.
[42] Foroutan M, Zamanpour I, Manafian J. Applications of IBSOM and ETEM for solving the nonlinear chains of atoms with long-range interactions. Europ Phys J Plus. 2017;132:1–18.
[43] Shakeel M, Liu X, Mostafa AM, AlQahtani NF, Alameri A. Dynamic Solitary Wave Solutions Arising in Nonlinear Chains of Atoms Model. J Nonl Math Phys. 2024;31(1):70.
[44] Junaid-U-Rehman M, Kudra G, Awrejcewicz J. Conservation laws, solitary wave solutions, and lie analysis for the nonlinear chains of atoms. Sci Rep. 2023;13(1):11537.
[45] Junaid-U-Rehman M, Kudra G, Awrejcewicz J. Conservation laws, solitary wave solutions, and lie analysis for the nonlinear chains of atoms. Sci Rep. 2023;13(1):11537.
[46] Junaid-U-Rehman M, Kudra G, Awrejcewicz J. Conservation laws, solitary wave solutions, and lie analysis for the nonlinear chains of atoms. Sci Rep. 2023;13(1):11537.
[47] Shakeel M, Liu X, Mostafa AM, AlQahtani NF, Alameri A. Dynamic solitary wave solutions arising in nonlinear chains of atoms model. J Nonl Math Phys. 2024;31(1):70.
[48] Ceesay B, Ahmed N, Maciiias-Diiiaz JE. Construction of M-shaped solitons for a modified regularized long-wave equation via Hirota's bilinear method. Open Phys 2024;22(1):20240057.
[49] Yang XF, Wei Y. Bilinear equation of the nonlinear partial differential equation and its application. J Funct Spaces. 2020;2020(1):4912159.
[50] Wazwaz AM. The Hirota's direct method and the tanh-coth method for multiple-soliton solutions of the Sawada-Kotera-Ito seventh-order equation. Appl Math Comput. 2008;199(1):133–8.
[51] Rizvi ST, Seadawy AR, Nimra Ahmad A. Study of lump, rogue, multi, M shaped, periodic cross kink, breather lump, kink-cross rational waves and other interactions to the Kraenkel-Manna-Merle system in a saturated ferromagnetic material. Opt Quantum Electron. 2023;55(9):813.

[52] Khan MH, Wazwaz AM. Lump, multi-lump, cross kinky-lump and manifold periodic-soliton solutions for the (2+1)-D Calogero–Bogoyavlenskii–Schiff equation. Heliyon 2020;6(4):e03701.
[53] Wang M, Tian B, Qu QX, Zhao XH, Zhang Z, Tian HY. Lump, lumpoff, rogue wave, breather wave and periodic lump solutions for a (3+1)-dimensional generalized Kadomtsev-Petviashvili equation in fluid mechanics and plasma physics. Int J Comput Math. 2020;97(12):2474–86.
[54] Zhao Z, Chen Y, Han B. Lump soliton, mixed lump stripe and periodic lump solutions of a (2+1)-dimensional asymmetrical Nizhnik-Novikov-Veselov equation. Modern Phys Lett B. 2017;31(14):1750157.
[55] Ren B, Lin J, Lou ZM. A new nonlinear equation with Lump-Soliton, Lump-Periodic, and Lump-Periodic-Soliton solutions. Complexity. 2019;2019(1):4072754.
[56] Rizvi STR, Seadawy AR, Ashraf MA, Bashir A, Younis M, Baleanu D. Multi-wave, homoclinic breather, M-shaped rational and other solitary wave solutions for coupled-Higgs equation. Europ Phys J Special Topics. 2021;230(18):3519–32.
[57] Ceesay B, Baber MZ, Ahmed N, Akgül A, Cordero A, Torregrosa JR. Modelling symmetric ion-acoustic wave structures for the BBMPB equation in fluid ions using Hirota's bilinear technique. Symmetry. 2023;15(9):1682.
[58] Tedjani AH, Seadawy AR, Rizvi ST, Solouma E. Dynamical structure and soliton solutions galore: investigating the range of forms in the perturbed nonlinear Schrödinger dynamical equation. Opt Quant Electron. 2024;56(5):764.
[59] Ozsahin DU, Ceesay B, Baber MZ, Ahmed N, Raza A, Rafiq M, et al. Multiwaves, breathers, lump and other solutions for the Heimburg model in biomembranes and nerves. Sci Rep. 2024;14(1):10180.
[60] Isah MA, Yokus A, Kaya D. Exploring the influence of layer and neuron configurations on Boussinesq equation solutions via a bilinear neural network framework. Nonl Dyn. 2024;112:1–17.
[61] Ceesay B, Ahmed N, Baber MZ, Akgül A. Breather, lump, M-shape and other interaction for the Poisson-Nernst-Planck equation in biological membranes. Opt Quantum Electron. 2024;56(5):853.